AIAA JOURNAL
Vol. 43, No. 6, June 2005

Experiments on Streamline-Curvature Instability in Boundary Layers on a Yawed Cylinder

Naoko Tokugawa* and Shohei Takagi†
Japan Aerospace Exploration Agency, Tokyo 182-8522, Japan
and
Nobutake Itoh‡
Teikyo University, Tochigi 320-8551, Japan

Instability of the three-dimensional boundary layer on a yawed circular cylinder placed in a uniform flow is investigated experimentally by introducing acoustic disturbances from a point near the attachment line. To exemplify the flow dominated by streamline-curvature instability rather than crossflow instability, which has been often observed in many swept-wing flows, is the aim here. In upstream regions of the disturbance wedge originating from the point source, both streamline-curvature and crossflow disturbances are superposed on each other and yield complicated amplitude distributions. A newly proposed method enables the decomposition of the distorted amplitude distribution into contributions from the two instability modes. Detailed observations, however, show that the crossflow mode decays with the distance from the source much faster than the streamline-curvature mode and allows the latter to be dominant in a region further downstream. A fundamental characteristic of the streamline-curvature instability wave is confirmed by examining its phase distribution in the spanwise and normal directions. Wave numbers and spatial growth rates are in good agreement with theoretical predictions.

Nomenclature

A	=	spanwise amplitude distribution
$\bar{A}$	=	spanwise total amplitude distribution
a	=	total wave function
C	=	inclination of phase
D	=	cylinder diameter
f	=	dimensional frequency
L	=	streamwise length
l_s	=	surface length
m	=	Falkner–Skan parameter
N	=	spatial growth rate of disturbance
Q	=	streamwise (parallel to the local external streamline) local velocity
q'	=	fluctuation of streamwise local velocity
Re_Q	=	uniform-flow Reynolds number
Re_δ	=	local Reynolds number
t	=	time
U	=	chordwise local velocity
u'	=	fluctuation of chordwise local velocity
V	=	spanwise local velocity
X	=	nondimensional chordwise (normal to the attachment line) distance from the attachment line along the surface
x	=	dimensional chordwise distance
Y	=	nondimensional spanwise (parallel to the attachment line) distance from the disturbance source
Y_0	=	nondimensional spanwise location where amplitude becomes maximum
Z	=	nondimensional radial (normal to the surface) distance from the surface
α_r	=	chordwise wave number of disturbance
β_r	=	spanwise wave number of disturbance
$\Delta\varphi$	=	phase difference between crossflow and streamline-curvature modes
δ	=	boundary-layer thickness
δ_{99}	=	boundary-layer thickness where streamwise local mean velocity Q is 99% of edge velocity Q_e
Λ	=	sweep angle
λ	=	wave length
ν	=	kinematic viscosity
σ	=	standard deviation of amplitude distribution
φ	=	spanwise phase of disturbance
φ_0	=	offset of phase
$\bar{\varphi}$	=	spanwise total phase distribution
Ψ	=	phase modulation
ω	=	angular frequency
$\hat{\omega}$	=	nondimensional frequency

Subscripts

CF	=	crossflow mode
e	=	local edge
SC	=	streamline-curvature mode
ω	=	component with angular frequency ω
∞	=	uniform flow

Presented as Paper 99-0814 at the AIAA 37th Aerospace Sciences Meeting, Reno, NV, 11–14 January 1999; received 9 November 2001; accepted for publication 16 November 2004.

*Associate Senior Researcher, Aerodynamics Research Group, Chofu.
†Director, Aerodynamics Research Group, Chofu. Senior Member AIAA.
‡Professor, School of Science and Engineering, Utsunomiya.

Introduction

THREE-DIMENSIONAL boundary layers are susceptible to two kinds of instabilities. One is the well-known crossflow (referred to as C-F) instability, which is of the inflection-point type and governs the process of laminar-to-turbulent transition in most cases.[1–3] The other is the streamline-curvature (S-C) instability, which is of the centrifugal type caused by the curvature of the flowfield in the plane parallel to the wall, as recently shown by a linear stability theory.[4–8]

In the flow on a rotating disk, the S-C instability has a very low critical Reynolds number and is amplified upstream of the critical point of C-F mode.[6] On the other hand, Takagi et al.[9] and Takagi and Itoh[10] have observed that amplified S-C disturbances directly influence spatial growth rate of C-F mode. It is also observed that strongly amplified S-C mode leads to another route of transition that is different from the usual process governed by C-F streamwise vortices.[9]

At the present stage, however, the S-C instability in boundary layers on swept wings is not well understood because the phenomenon has been ignored or unrecognized until the recent theoretical prediction by Itoh[4–7] and the subsequent experimental confirmation by Takagi et al.[11] Because of its potential significance to transition, it is highly desirable to investigate experimentally the role of the S-C instability in the transition process of swept-wing boundary layers.

As a first step in such investigations, the present study is directed to the problem of whether or not the S-C disturbances can have a magnitude comparable to or larger than the C-F mode in a simple three-dimensional boundary layer. Fortunately, a linear stability theory has predicted some geometrical conditions under which the S-C mode is unstable, but the C-F mode is always stable in the flow on a swept cylinder.[7] An artificial excitation is made to clarify stability characteristics of the flow by introducing an acoustic disturbance through a tiny hole near the leading edge of the cylinder.

Outline of Theoretical Prediction

Linear stability theory predicts that the three-dimensional boundary layer on a yawed circular cylinder experiences multiple instabilities such as attachment-line instability, streamline-curvature instability and crossflow instability, and their critical Reynolds numbers are susceptible to experimental conditions such as geometric configurations and chordwise locations. With a parametric study focusing on this susceptibility, Itoh[7] provides a guide to enhance the streamline-curvature mode. This guide is used to determine the experimental configuration presented here and to identify the experimentally observed disturbances as S-C mode or C-F mode. This section provides a brief outline of the theoretical approach and the computational results.

Boundary-layer velocity distributions necessary for stability analysis are described with members of Falkner–Skan–Cooke velocity family subject to an approximate method of boundary-layer calculations. The stability equations used include two curvature terms of wall and external streamline as well as a nonparallel term to compensate the boundary-layer growth. The method of complex characteristics is employed to predict pathlines of the disturbance developing from a point source. More details are given by Itoh.[7]

Orthogonal curvilinear coordinates are used on the surface of the circular cylinder in chordwise (normal to the attachment line), spanwise (parallel to the attachment line), and radial (normal to the surface) directions and are denoted by X, Y, and Z, respectively (Fig. 1). The circumferential distance X from the attachment line and the spanwise distance Y from the point source have been normalized with the surface length $l_s = \pi D/2$, but the distance Z from the surface has been scaled with the boundary-layer thickness $\delta = \sqrt{[\nu m/(\mathrm{d}U_e/\mathrm{d}x)]}$. The Falkner–Skan parameter $m(X)$ is determined as a solution of the momentum integral equation in

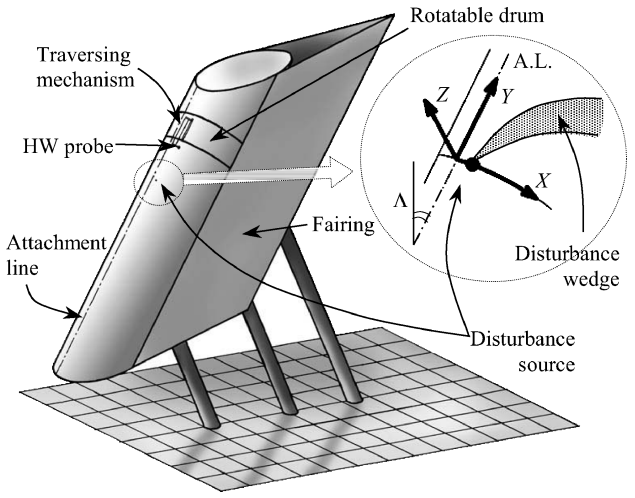

Fig. 1 Swept cylinder model in the low-speed wind tunnel and schematic of the flowfield and coordinates.

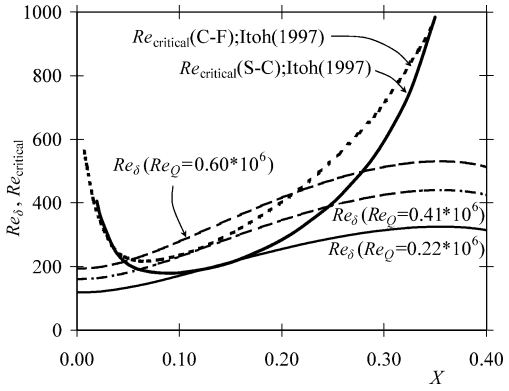

Fig. 2 Theoretically obtained critical curves of S-C and C-F modes and local Reynolds numbers for various uniform-flow Reynolds numbers.

the direction normal to the leading edge. The two characteristic lengths used in nondimensionalization define two Reynolds numbers as the uniform-flow Reynolds number $Re_Q = Q_\infty L/\nu$ and the local Reynolds number $Re_\delta = Q_e\delta/\nu$. Here $L = D/\cos\Lambda$, $Q_e = \sqrt{(U_e^2 + V_e^2)}$, $U_e = 2Q_\infty \cos\Lambda \times \sin(\pi X)$, $V_e = Q_\infty \sin\Lambda$, and Q_∞ is the uniform-flow velocity.

The critical Reynolds numbers obtained for both C-F instability and S-C instability vary in a parabolic shape with the circumferential distance X from the attachment line and have minimum values in a middle range of X. Results given in Fig. 2 indicate the S-C mode is predicted to have a lower critical Reynolds number than the C-F mode. In the case of a sweep angle $\Lambda = 30$ deg, the difference in the critical Reynolds number between the two modes seems to be maximized, so that the S-C mode will dominate a large part of the cylinder except for a very narrow region near the attachment line. It is shown that when the Re_Q is so high as about 0.6×10^6 both modes of disturbances grow because then Re_δ exceeds the two critical values. When Re_Q is approximately 0.4×10^6, however, the local Reynolds number locates above the critical curve of S-C mode in the region between $X \cong 0.06$ and 0.25 but always below that of C-F mode. Thus S-C disturbances are expected to grow, whereas C-F disturbances are subjected to decay everywhere in the three-dimensional boundary layer on a circular cylinder under the conditions of $\Lambda = 30$ deg and $Re_Q = 0.4 \times 10^6$. This situation meets our purpose of creating the flow dominated by the S-C mode.

When artificial disturbances are introduced into the boundary layer from a point near the attachment line, amplifying disturbances develop into a wedge-shaped distribution extending to the downstream direction because of their dispersive properties. An integration of the amplified disturbances along their propagation path yields the spatial growth rate N as a function of the spanwise wave number β_r and the frequency f of disturbances. Spanwise distribution of N forms a bump with the peak at $\hat{\omega} \equiv 2\pi f \cdot L/(Q_\infty\sqrt{Re_Q}) = -0.06$, where the negative sign of frequency means that a constant-phase line propagates in the direction opposite to the wave-number vector. Disturbances with negative frequency belong to S-C mode and propagate in the inward direction of external streamlines, whereas C-F disturbances consist of positive frequencies and propagate toward the convex side of the streamlines in most cases. Thus we can distinguish the two modes by examining the temporal variation of the phase distribution along the spanwise coordinate Y in our experiments. The phase distribution in the direction normal to the surface is another important property for identification of the instabilities because there is a conspicuous difference between S-C and C-F modes; that is, the difference between maximum and minimum values of the phase is about 45 deg for S-C mode but is three times larger than it for C-F mode.

Experimental Arrangement and Procedure

Wind Tunnel

The low-speed wind tunnel (LWT1) and the calibration wind tunnel (CWT) at Japan Aerospace Exploration Agency were used throughout the series of experiments.

The LWT1 is of the closed-circuit type and has a test section of 5.5 m in width, 6.5 m in height and 9 m in length, the cross-sectional shape of which is modified to be octagonal to prevent secondary flow. The static pressure in the test section is maintained at atmospheric value through a breather 0.5 m in width between the exit of the test section and the collector of the return section. Upstream of the test section, there is a nozzle with a contraction ratio of 5.3, and a screen of 30 mesh is installed in the settling chamber to reduce freestream turbulence. The velocity in the test section is attainable up to the maximum 70 m/s by changing the rotating speed of the fan blades. The turbulence level is about 0.14% at a velocity of 10 m/s and increases with velocity.[12] This level includes both vortical and acoustic fluctuations, but measurements by a microphone in the flow indicate 79 dB the acoustic noise level only at the same velocity.[12]

The CWT is also a closed circuit with a rectangular test section of 0.55 m in width, 0.65 m in height and 1.5 m in length. Streamwise pressure gradient in the test section is prevented by flare of the floor and the ceiling. The nozzle upstream of the test section has a contraction ratio of 9, and a honeycomb and five identical screens with 20 mesh are installed to reduce freestream turbulence in the settling chamber. The maximum velocity is 65 m/s, and the turbulence level is 0.06% including acoustic noise level of 98 dB at the velocity of 30 m/s (Ref. 12).

The LWT1 is more suitable for transition measurements than the CWT because a thicker boundary layer develops on a larger model. Under the condition of $Re_Q = 0.22 \times 10^6$, for instance, the boundary-layer thickness based on the relation $\delta_{99} = 3.055 \times \delta$, is 1.86 mm on the attachment line in LWT1, which is much smaller than $\delta_{99} = 0.37$ mm in the CWT, where $\delta(X = 0) \equiv (\nu D/4Q_\infty \cos\Lambda)^{1/2}$. Thus the majority of the experiment was conducted at LWT1, and the principal results were confirmed at CWT where turbulence level is much lower than LWT1.

Cylinder Models and Traversing Mechanism

Two models were prepared for the series of experiments. The one for LWT1 is made of a steel pipe with an external diameter of 500 mm and length of 3.6 m, and flat plywood boards were attached on the leeward side of the cylinder to prevent mechanical vibration owing to vortex shedding from the cylindrical part, so that total chordwise length was extended to 1220 mm measured from the attachment line. The model was supported up from the floor to be set at a sweep angle of 30 deg. Its whole surface of the cylindrical part was carefully machined and finished in flat-black coating. A tiny hole with a diameter 0.5 mm was opened to introduce artificial disturbances by the use of a loud speaker installed inside the cylinder. The hole is located at 20.4 deg ($X = 0.11$ in nondimensional form) from the attachment line and 2170 mm from the windward tip. A part of the cylinder constructs a drum rotatable around the axis, the surface being kept flush to the cylinder surface. This drum is used for hot wire traversing in the chordwise direction X, and other three traversing mechanisms are installed inside the drum for the Z direction normal to the surface, for the spanwise Y direction, and for rotation of hot-wire sensor around the center of its supports. All four motions are independently driven by four stepping motors managed under a 16-bit microcomputer.

The other circular-cylinder model for CWT is made of stainless steel with an external diameter of 100 mm and a spanwise length of 577 mm and with the whole surface also carefully machined. Aluminum flat plates were attached on the leeward region of the cylinder, forming a total chordwise length of 197 mm from the attachment line. The two ends of cylinder were cut so as to be parallel to the uniform flow, when the model was horizontally set at a sweep angle of 30 deg in the middle of the test section. Both ends were 50 mm apart from the sidewalls to avoid oncoming boundary-layer contamination and blockage effect. A tiny hole with an internal diameter of 0.1 mm for introducing the disturbance is opened at $X = 0.10$ and 250 mm from the upward tip, and a loud speaker was installed just underneath the hole. The traversing systems in streamwise, vertical, and transverse directions are installed in the wind tunnel with a carriage above the ceiling of the test section. Movement of the hot-wire sensor is controlled by independent stepping motors managed by a 32-bit microcomputer.

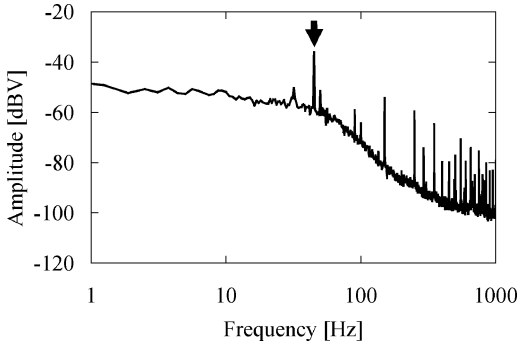

Fig. 3 Typical spectrum measured at $Re_Q = 0.22 \times 10^6$, in which a component of exciting frequency 45 Hz has an appropriate amplitude.

Hot-Wire Anemometer and Data Reduction

A tungsten wire of 5 μm in diameter and 1 mm in length with copper-plated sleeves at both ends was soft-welded on the tips of the prong support. The rotation angle of hot-wire sensor was adjusted to be normal to local external flow at each position of X at LWT1, whereas the hot-wire axis was fixed to be inclined parallel to the attachment line at CWT. The hot-wire anemometer was operated in constant temperature mode, and the output of the CTA bridge was linearized in an analog circuit, with the linearizer output separated into the mean and fluctuating velocities. The roll-off frequency of the system was higher than 20 kHz. The mean velocity was recorded by analog XY pen recorder together with the position of hot-wire sensor, which was supplied from D/A board installed in the microcomputer managing the traversing mechanism just described. The fluctuating velocity was analyzed by a 16-bit fast-Fourier-transform analyzer.

Experimental Procedure

The monochromatic disturbance of nondimensional frequency $|\hat{\omega}| = 0.06$ was introduced through a hole at $X \cong 0.1$ by the use of a loud speaker, except for the case of mean velocity measurements. In the case of artificial forcing the main effort was made to measure the magnitude and phase of growing disturbances with the forcing frequency, which were obtained from spectral analysis as shown in Fig. 3 and from the cross-correlation function between observed disturbances and the forcing signal. Hot-wire measurements were made in the wedge-shaped disturbance region developing from a source point, and the hot-wire sensor was traversed in the spanwise direction Y at a certain chordwise station X. A hot wire was held fixed at the height Z, where unsteady disturbance has the maximum amplitude in each distribution normal to the surface, roughly corresponding to 80% of the local boundary-layer edge velocity Q_e.

Hot-Wire Survey in the Upstream Region

Mean-Velocity Profile on the Attachment Line

Experiments were begun with measurement of the laminar flow on the attachment line because it was first necessary to confirm that the basic flow was completely free from the attachment-line contamination sometimes coming from the boundary layer on the wind-tunnel wall or from the upstream tip of the cylindrical model. Mean-velocity profiles just on the attachment line were obtained for uniform-flow velocities $Q_\infty = 6$, 11, and 16 m/s, corresponding to $Re_Q = 0.22 \times 10^6$, 0.41×10^6, and 0.60×10^6, respectively, and are compared with the theoretical profile[13] as shown in Fig. 4. All velocities measured at different values of Re_Q fall nearly on a single curve and indicate very good agreement with the theory, except for a limited region near the wall, where hot-wire measurements are suffered from inevitable thermal interactions between hot-wire and metallic surface. Thus it can be considered that the boundary layer in this experiment is laminar and can be justifiably approximated with the theoretical prediction for an infinitely long yawed cylinder.

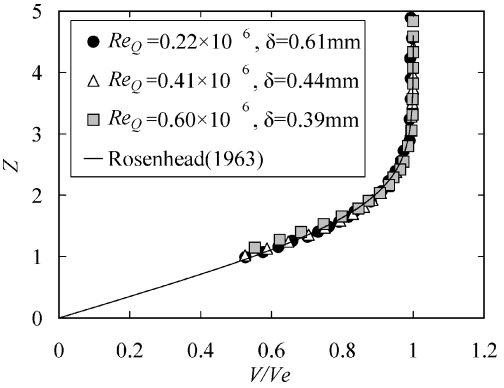

Fig. 4 Boundary-layer profiles on the attachment line at three different uniform-flow Reynolds numbers of $Re_Q = 0.22 \times 10^6$, 0.41×10^6, and 0.60×10^6.

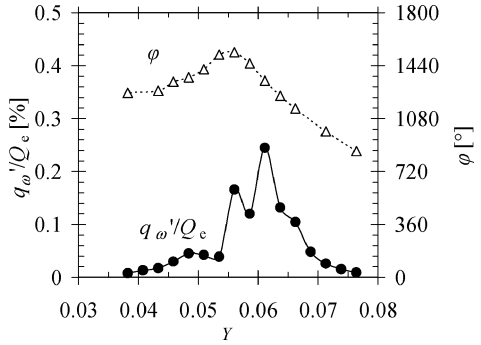

Fig. 5 Amplitude (q'_ω/Q_e) and phase distributions (φ) of $Re_Q = 0.41 \times 10^6$ and $|\hat{\omega}| = 0.06$ at $X = 0.21$ plotted against spanwise coordinate Y.

Disturbance Development in an Unstable Region

Theoretical computations just outlined indicate that S-C disturbances are amplified between $X \cong 0.06$ and 0.25, for a uniform-flow Reynolds number of $Re_Q = 0.41 \times 10^6$. Following this prediction, the first experiment on the wedge-shaped disturbances was made at the same value of Re_Q and by introducing a sound disturbance of the frequency 105 Hz from a hole at $X = 0.11$, which corresponds to the nondimensional frequency $|\hat{\omega}| = 0.06$. Hot-wire observations of the resulting velocity fluctuations were made at $X = 0.21$ by traversing the disturbance wedge in the spanwise direction. Figure 5 shows the amplitude and phase of the wavy fluctuations plotted against the spanwise coordinate Y. The phase distribution consists of two nearly straight lines with positive and negative slopes, showing that there are two kinds of wavy disturbances propagating in opposite directions to each other because the sign of slope indicates the direction of phase velocity. The disturbances with positive slope in the left-hand region $Y < 0.0535$ have phase velocities to the inward direction of curved external streamlines and therefore can be identified as those arising from the S-C instability according to theoretical prediction. On the contrary, the phase distribution on the right-hand side ($Y > 0.0586$) has a negative slope, so that the disturbances appearing in this region are presumed to come from the C-F instability, whose disturbances usually propagate toward the convex side of streamlines. These results of phase measurements indicate that the disturbance wedge developing from a point source surely consists of both S-C instability on the left-hand side and C-F instability on the right-hand side.

Next we turn our attention to the amplitude distribution also given in Fig. 5, which has a much more complicated feature than the phase distribution just discussed. The amplitude distribution in the Y direction is highly modulated and has several peaks between both ends of the spanwise distribution, though it is naturally expected to have two peaks corresponding to the most amplified disturbances of the S-C and C-F instabilities. The most important features included in the results are an unexpectedly large amplitude for C-F disturbances

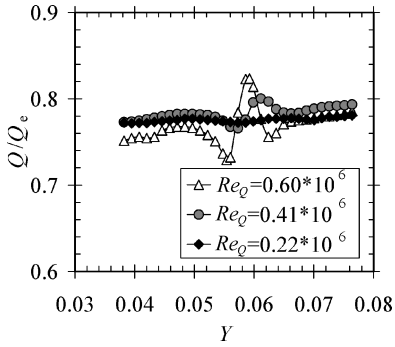

Fig. 6 Mean velocity distributions at $X = 0.21$ and at constant height Z plotted against spanwise coordinate Y of three uniform-flow Reynolds numbers.

and the appearance of more than two peaks in the amplitude distributions plotted against Y. The latter problem should be discussed at first because the presence of at least three major peaks in the amplitude distribution prevents us from determining individual magnitude of the S-C and C-F disturbances. This multipeak structure of amplitude distribution is common not only to this measurement but also to results of similar experiments performed at different magnitudes of initial amplitude and at different sweep angles.[11,14]

Influence of Stationary Vortices

The amplitude modulation just mentioned can be produced by stationary vortices, which are usually observed in a boundary layer dominated by the crossflow instability. This is deduced because the location of strong modulation near the center of wedge width almost meets the location of stationary vortices, which is generally between the region of S-C traveling waves on the left-hand side and that of C-F traveling waves on the right-hand side. For more details, spanwise distributions of the mean velocity at a constant height were measured under the same experimental conditions as already discussed, and the results are given in Fig. 6, which surely indicates the presence of weak streamwise vortices in the mean-velocity field. The question is, therefore, how the stationary vortices are related to the amplitude modulation of our concern, and whether such weak vortices can yield such marked distortion of the amplitude distribution.

To investigate this correlation, further observations of both steady and unsteady disturbances were made at two different uniform-flow velocities $Q_\infty = 6$ and 16 m/s and with excitation frequencies of 45 and 210 Hz, respectively, which correspond to the uniform-flow Reynolds numbers $Re_Q = 0.22 \times 10^6$ and 0.60×10^6 together with the nondimensional frequency $|\hat{\omega}| = 0.06$. Figure 7 shows the spanwise distributions of disturbance amplitude and phase observed at $X = 0.21$ for comparison with the variation of mean-flow velocities with Y at the same streamwise stations given in Fig. 6. It can be seen that the magnitude of stationary vortices increases with Re_Q but that the modulation of amplitude distribution is weakened as Re_Q increases. The amplitude modulation remains even if the stationary vortices almost vanish. Thus we can conclude that the multipeak structure in the spanwise amplitude distribution is not caused by streamwise stationary vortices.

Simple Superposition of Two Wavy Disturbances

As already stated, each of the amplitude distributions given in Figs. 5 and 7 seems to consist of three major peaks, that is, two peaks coming from the maximum S-C and C-F disturbances and an additional one between these two peaks. This suggests a strong possibility that the third peak can result from simple superposition of the two original peaks on both sides. Because the S-C and C-F disturbances have different phase distributions, the resulting amplitude can presumably vary with the spanwise distance in a very complicated manner. As a matter of fact, similar amplitude distortions were observed at different sweep angles in other series of experiments[11,14] and reproduced by a direct numerical simulation using the Navier–Stokes equations.[15,16] In the process of analyzing

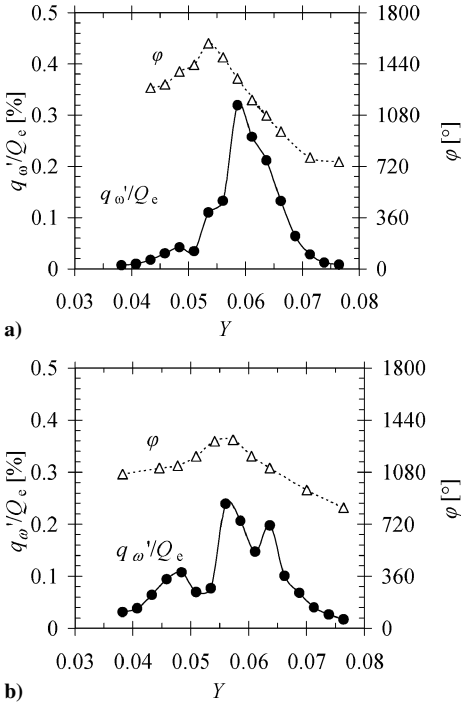

Fig. 7 Amplitude and phase distributions in the direction of the spanwise coordinate Y ($|\hat{\omega}| = 0.06$): a) $Re_Q = 0.60 \times 10^6$ at $X = 0.21$, and b) $Re_Q = 0.22 \times 10^6$ at $X = 0.21$.

those data, a simple method has been proposed[17] to decompose measured amplitude distribution numerically to two independent distributions coming from the S-C and C-F modes. In the following, the decomposition method is outlined and applied to the present problem to show modulation can occur by a simple superposition of two modes.

At first, let the disturbances of S-C and C-F instabilities be approximated by simple sinusoidal waves, $A_{SC}(Y)\cos[\omega t + \varphi_{SC}(Y)]$ and $A_{CF}(Y)\cos[\omega t + \varphi_{CF}(Y)]$, which have the same angular frequency ω but whose amplitudes and phases can independently vary with the spanwise coordinate Y. Then superposition of the two waves yields

$$a(Y,t) = A_{SC}(Y)\cos[\omega t + \varphi_{SC}(Y)] + A_{CF}(Y)\cos[\omega t + \varphi_{CF}(Y)]$$
$$= \bar{A}(Y)\cos[\omega t + \varphi_{SC}(Y) + \Psi(Y)]$$

where $\bar{A} = (A_{SC}^2 + A_{CF}^2 + 2A_{SC}A_{CF}\cos\Delta\varphi)^{(1/2)}$, $\Psi = \tan^{-1}[A_{CF}\sin\Delta\varphi/(A_{SC} + A_{CF}\cos\Delta\varphi)]$, and $\Delta\varphi(Y) = \varphi_{CF} - \varphi_{SC}$. The most important result is that the time-averaged amplitude $\bar{A}(Y)$ of the resulting waves depends on the phase difference $\Delta\varphi(Y)$ between the two instability waves. If the original amplitudes A_{SC} and A_{CF} are of comparable magnitude and the phase difference $\varphi_{CF} - \varphi_{SC}$ is not negligibly small, then very sharp variation of $\bar{A}$ with Y is possible and can sometimes be accompanied by several peaks and valleys.

In the decomposition method developed by the present authors,[17] the shapes of original amplitude and phase distributions for each mode are assumed to be written in the form

$$A = \exp\frac{\left[-(Y - Y_0)^2/2\sigma^2\right]}{\left[(2\pi)^{(\frac{1}{2})}\sigma\right]}, \qquad \varphi = CY + \varphi_0$$

and two parameters, inclination C and constant term φ_0, are determined from the linear approximation of experimental data. Then the two parameters Y_0 and σ for each mode are obtained so as to minimize the difference between total amplitude $\bar{A}(Y)$ and experimentally measured distribution. Figure 8 shows the decomposed amplitude and phase distributions corresponding to the experimental data given in Fig. 5. A linear superposition of two wavy distributions coming from S-C and C-F instabilities clearly explains the existence of unexpected peaks in the amplitude distribution near the source point.

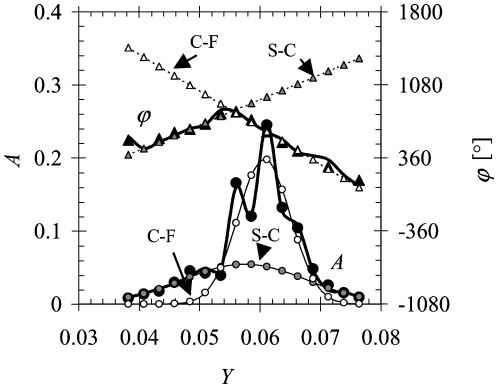

Fig. 8 Illustration of decomposed amplitude and phase distributions of $Re_Q = 0.41 \times 10^6$ and $|\hat{\omega}| = 0.06$ at $X = 0.21$: ▲, ●, experimental results; ▲, ●, decomposed S-C mode; △, ○, decomposed C-F mode; and ——, superposition of two modes.

As the result of the successful decomposition of two modes, it is found that the maximum amplitude of S-C instability is much smaller than that of C-F instability for the case of $Re_Q = 0.41 \times 10^6$ (Fig. 8), indicating the large growth of C-F mode in contrast with theoretical prediction. At the same location as Fig. 8 but at a different uniform-flow Reynolds number $Re_Q = 0.60 \times 10^6$ (Fig. 9a), the maximum amplitude of S-C mode also becomes smaller than that of C-F mode. However, decrease of the uniform-flow Reynolds number seems to increase relative magnitude of S-C mode (Fig. 9b). It is really found that the maximum amplitude of S-C instability becomes large and comparable with that of C-F instability at the slightly downstream location $X = 0.26$ (Fig. 9c). Downstream region is useful for observation of their independent properties because two modes will appear away from each other after their sufficient dispersion and under the decreasing influence of the superposition.

These results imply that S-C mode will dominate the flow in the condition of lower uniform-flow Reynolds number and at the downstream location. It is also important to turn our attention to the growth rate of S-C and C-F modes because the amplitudes of each mode cannot exactly be determined because of the uncertainty of their initial amplitude.

Flowfield Dominated by Streamline-Curvature Instability

The preceding investigation near the source point has shown that the disturbance wedge extending from a point source surely includes both S-C and C-F disturbances and that superposition of the two modes yields a very complicated variation of the disturbance amplitude in the spanwise direction. The highly modulated amplitude distribution observed at the earlier development seems to be caused by insufficient separation between the S-C and C-F modes of similar magnitudes after a short traveling distance from the source. These circumstances imply usefulness of extending the investigation into regions further downstream, where both S-C and C-F modes might tend to decay but their distinct separation enables us to determine their individual magnitudes in a definite manner. Thus an experiment on such a downstream region was performed at the CWT to obtain more reliable data for direct comparison with theoretical predictions. This wind tunnel is smaller in scale than LWT1 but is suitable for detailed investigations of instability waves because of its lower residual turbulence.

The experiment was made at the uniform-flow velocity $Q_\infty = 30$ m/s and with the excitation frequency $f = 1.1$ kHz, corresponding to $Re_Q = 0.22 \times 10^6$ and $|\hat{\omega}| = 0.06$, respectively. The point-source excitation was located at $X = 0.10$, and the hot-wire observations were at the two downstream stations $X = 0.45$ and 0.50. The principal results are shown in Fig. 10, where the observed amplitude and phase are plotted against the spanwise location Y. Each amplitude distribution has one major peak beside one almost invisible minor peak under the corresponding phase lines

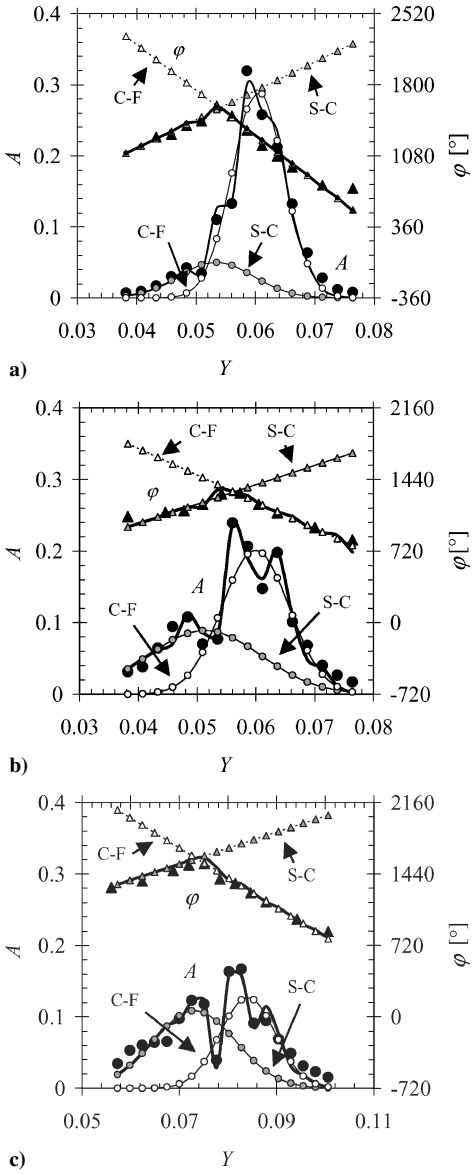

Fig. 9 Illustration of decomposed amplitude and phase distributions ($|\hat{\omega}| = 0.06$): a) $Re_Q = 0.60 \times 10^6$ at $X = 0.21$, b) $Re_Q = 0.22 \times 10^6$ at $X = 0.21$, and c) $Re_Q = 0.22 \times 10^6$ at $X = 0.26$ (▲, ●, experimental results; △, ○, decomposed S-C mode; △, ○, decomposed C-F mode; and ——, superposition of two modes).

oppositely inclined. Separation of the two peaks becomes more distinct as the downstream distance X increases, partly because the dispersive properties of the instability waves enlarge the difference of propagation paths and partly because spatial damping of all disturbances in the stable region makes each extent of the two peaks smaller (Fig. 2). The major peak is supposed to be S-C mode from its spanwise phase distribution. Such a distinct separation enables us to determine the maximum amplitude of S-C disturbances and to draw its variation with X.

The major peaks of amplitude distributions obtained at such downstream stations are judged to belong to S-C instability according to the phase distributions in the Y direction. For confirmation of this judgment, the amplitude and phase distributions across the boundary layer were measured at the peak location $Y = 0.144$ of $Re_Q = 0.22 \times 10^6$, $|\hat{\omega}| = 0.06$ and $X = 0.50$. The results presented in Fig. 11 include a certain scatter of phase near the second peak of a very small amplitude, but show the phase distribution of S-C mode in good agreement with the theoretical curve. It can thus be concluded that the large peak centered at $Y = 0.144$ is surely caused by the S-C instability.

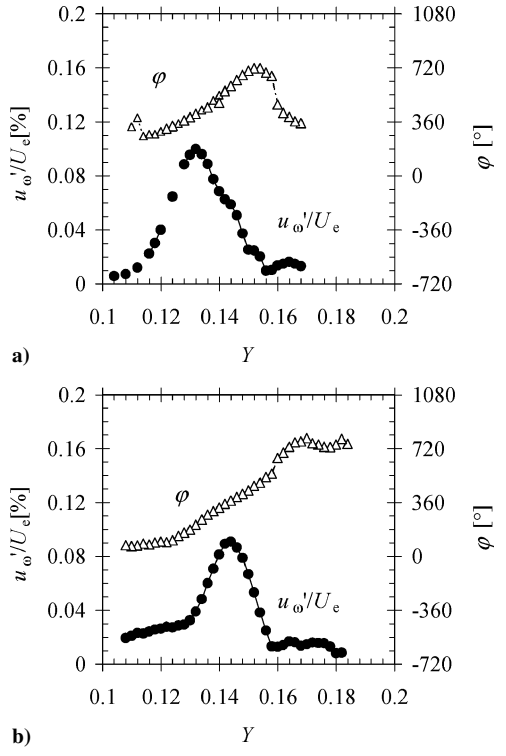

Fig. 10 Amplitude and phase distributions at the CWT of $Re_Q = 0.22 \times 10^6$ and $|\hat{\omega}| = 0.06$ in the direction spanwise coordinate Y at constant heights Z at a) $X = 0.45$ and b) $X = 0.50$.

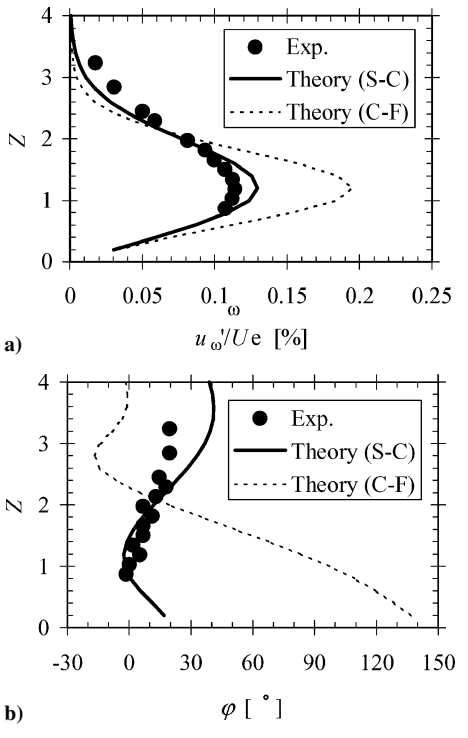

Fig. 11 Boundary-layer profiles at the major peak in the spanwise distribution in Fig. 10b of $Re_Q = 0.22 \times 10^6$ and $X = 0.50$: a) magnitude and b) phase.

The wavelength λ of S-C disturbances and the propagating direction $\tan^{-1}[\beta_r/a_r]$ from X axis were obtained by drawing isophase lines on the spanwise phase distributions, measured at $X = 0.45$, 0.475, and 0.5. The results given in Fig. 12a are in good agreement with theoretically predicted values. Finally, Fig. 12b gives the ratios of the amplitudes experimentally obtained at $X = 0.475$ and 0.5 to the amplitude at $X = 0.45$ and shows good agreement with the corresponding ratio of the theoretical values of N.

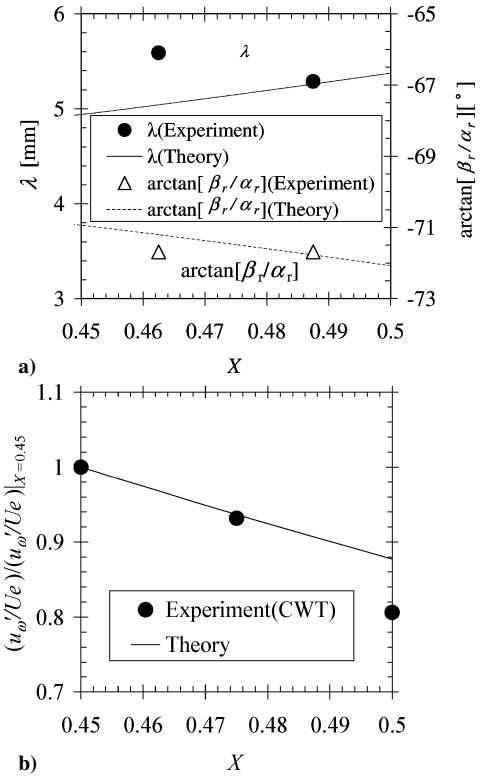

Fig. 12 Properties of S-C disturbances at the CWT of $Re_Q = 0.22 \times 10^6$ and $|\tilde{\omega}| = 0.06$: a) wavelength and propagating direction and b) growth rate relative to the one at $X = 0.45$.

Conclusions

Experimental investigations on a yawed circular cylinder have been made to show the existence of such a three-dimensional boundary layer that is dominated by the streamline-curvature disturbance, as predicted by a linear stability theory. The wedge-shaped disturbance developing from a point source actually consists of both S-C and C-F modes, though the amplitude distribution is highly modulated in the unstable region just behind the point source. A simple mathematical model shows that superposition of two instability waves with different phase distributions yields this kind of complicated modulations of amplitude and that the modulated amplitude distribution is decomposable into two independent distributions. The decomposed distributions show C-F disturbances with an unexpectedly large amplitude at higher uniform-flow Reynolds numbers, though it becomes relatively smaller at lower uniform-flow Reynolds numbers. In a further downstream region, however, the amplitude distribution at a comparatively low Reynolds number is smoothed to have two distinct peaks because the influence of superposition decreases because of a rapid decay of the C-F mode and the dispersive separation of the two modes. The disturbances observed at the two major peaks are identified as S-C and C-F instabilities by comparing their phase distributions in the direction normal to the surface with theoretical curves. The amplitude ratio of S-C mode to C-F mode increases as the chordwise distance X increases, and the flow is dominated by S-C disturbances in the final stage of observation at $X = 0.5$, where the flow is stable only with very small decaying disturbances. Characteristics of the S-C mode, such as wavelength, propagating direction, and growth rate, are found to be in good agreement with theoretical prediction because of no influence of C-F disturbances there. It should be noted that all of the experiments reported here observed C-F disturbances with a magnitude larger than, or at least comparable to, the magnitude of S-C disturbances, except for the far downstream region around $X = 0.5$. This is inconsistent with the theoretical prediction that there is a flow whose local Reynolds numbers are above the S-C critical curve but below the C-F critical one. The reason might be that the difference in critical values between S-C and C-F modes is not so large as to be reflected in their practical development. Slightly different neutral curves will be obtained from different theoretical models. In fact, the new model equation[8] predicts a lower critical value of C-F instability than that of S-C instability, in contrast to the theoretical prediction explained earlier. The other possibility for the inconsistency with the theoretical prediction is that initial amplitudes created near the source point are not the same for all wave-number components. The receptivity of S-C and C-F modes should be examined to clarify the reason why C-F mode is much larger than theoretical prediction near the source.

Acknowledgments

The authors express their cordial appreciation to A. Nishizawa, Japanese Aerospace Exploration Agency, for helpful discussion and G. A. Buck, South Dakota School of Mines and Technology, for his proofreading.

References

[1]Reed, H. L., and Saric, W. S., "Stability of Three-Dimensional Boundary Layers," *Annual Review of Fluid Mechanics*, Vol. 21, 1989, pp. 235–284.

[2]Takagi, S., and Itoh, N., "Observation of Traveling Waves in the Three-Dimensional Boundary Layer Along a Yawed Cylinder," *Fluid Dynamics Research*, Vol. 14, No. 4, 1994, pp. 167–189.

[3]Takagi, S., and Itoh, N., "Dispersive Evolution of Crossflow Disturbances Excited by an Airjet Column in a Three-Dimensional Boundary Layer," *Fluid Dynamics Research*, Vol. 22, No. 1, 1998, pp. 25–42.

[4]Itoh, N., "Instability of Three-Dimensional Boundary Layers Due to Streamline Curvature," *Fluid Dynamics Research*, Vol. 14, No. 6, 1994, pp. 353–366.

[5]Itoh, N., "Development of Wedge-Shaped Disturbances Originating from a Point Source in a Three-Dimensional Boundary Layer," *Fluid Dynamics Research*, Vol. 18, No. 6, 1996, pp. 337–354.

[6]Itoh, N., "Simple Cases of the Streamline-Curvature Instability in Three-Dimensional Boundary Layers," *Journal of Fluid Mechanics*, Vol. 317, 1996, pp. 129–154.

[7]Itoh, N., "Instability Waves Developing from a Point Source near the Attachment-Line on a Yawed Circular Cylinder," *Transactions of the Japan Society for Aeronautical and Space Sciences*, Vol. 39, No. 126, 1997, pp. 428–441.

[8]Itoh, N., "Multi-Instability Analysis of Swept-Wing Boundary Layers Part. 1 A Nonparallel Model of Stability Equations," *Transactions of the Japan Society for Aeronautical and Space Sciences*, Vol. 45, No. 149, 2002, pp. 195–201.

[9]Takagi, S., Itoh, N., and Tokugawa, N., "Characteristics of Streamline-Curvature Disturbances in a Rotating-Disk Flow," AIAA Paper 98-0341, Jan. 1998.

[10]Takagi, S., and Itoh, N., "Characteristics of Unsteady Disturbances due to Streamline-Curvature Instability in a Rotating-Disk Flow," *Proceedings of the Seventh Asian Congress of Fluid Mechanics*, Vol. 1, edited by R. Narasimha, Allied Publishers, Delhi, India, 1997, pp. 187–190.

[11]Takagi, S., Itoh, N., and Tokugawa, N., "Dispersive Growth of Unsteady Disturbances due to Cross-Flow and Streamline-Curvature Instabilities in 3-D Boundary Layers," *Abstracts of 19th ICTAM*, 1996, p. 199.

[12]Tokugawa, N., Takagi, S., Atobe, T., Ido, A., and Kohama, Y., "Influence of the External Disturbances on Natural Boundary-Layer Transition in 2-D Wing Flows," *Nagare*, Vol. 22, No. 6, 2003, pp. 485–498 (in Japanese).

[13]Rosenhead, L., *Laminar Boundary Layers*, Oxford Univ. Press, Oxford, 1963, Chap. 8.

[14]Prijo, K., Takagi, S., Tokugawa, N., Itoh, N., and Nishizawa, A., "Behavior of Unsteady Disturbances near the Attachment Line," *Proceedings of NAL Workshop on Laminar-Turbulent Transition in Boundary Layers*, NAL SP-48T, 2001, pp. 21, 22.

[15]Yokokawa, Y., and Fukunishi, Y., "Numerical Study on the Characteristics of Instability Waves in a Crossflow Boundary Layer," *Proceedings of NAL Workshop on Laminar-Turbulent Transition in Boundary Layers*, NAL SP-48T, 2001, pp. 25–28.

[16]Inasawa, A., Izawa, S., Xiong, A. K., and Fukunishi, Y., "Growth of a Point Source Disturbance Introduced into the Three-Dimensional Boundary Layer of a Yawed Cylinder," *Proceeding of the Tenth Asian Congress of Fluid Mechanics* [CD-ROM], edited by J. J. Wijetunge, Univ. of Peradeniya, Peradeniya, 2004.

[17]Tokugawa, N., Prijo, Kusumo, Nishizawa, A., and Takagi, S., "Decomposition of Two Kinds of Instability Waves in Three-Dimensional Boundary Layer near Yawed Attachment Line," *Nagare Multimedia*, 2002 (in Japanese), URL: http://www.nagare.or.jp/mm/2002/tokugawa/index.htm [cited 25 December 2002].

P. R. Bandyopadhyay
Associate Editor